Nigerian Research Journal of Engineering and Environmental Sciences 5(2) 2020 pp. 591-601

Nigerian Research Journal of Engineering and Environmental Sciences
Journal homepage: www.rjees.com

Original Research Article

A Comparative Study of Subsurface Earth Classification Between Two Dimensional and Three Dimensional Geoelectrical Imaging in University of Benin Teaching Hospital, Benin City, Nigeria

***Avenbuan, N., Alile, O.M. and Iduseri, O.M.**

Department of Physics, Faculty of Physical Sciences, University of Benin, PMB 1154, Benin City, Nigeria.
*avenbuannosayaba@yahoo.com

ARTICLE INFORMATION

Article history:
Received 24 Sep, 2020
Revised 17 Oct, 2020
Accepted 29 Oct, 2020
Available online 30 Dec, 2020

Keywords:
Resistivity
Two-dimensional (2D)
Three-dimensional (3D)
False anomaly
Inversion model
Imaging plane

ABSTRACT

The two-dimensional (2D) and three-dimensional (3D) geoelectrical methods of exploration are mostly used in complex and inhomogeneous subsurface media. In a 2D inversion program, the earth is assumed to have a 2D resistivity distribution. However, the resistivity distribution of the earth is inherently 3D. To establish the similarities and dissimilarities between these two survey methods, data were obtained along parallel and orthogonal lines using the Wenner-Schlumberger Array configuration technique at the University of Benin Teaching Hospital Field, Benin City, Nigeria. A 3D data was obtained by combining series of 2D parallel and orthogonal data set using a batch file. The 2D orthogonal and parallel data set were processed using RES2DINV, while the resulting 3D data set was processed using RES3DINV software to obtain the 2D and 3D inversion results. The 3D inversion results were exported to a Voxler software where the volume image of the subsurface was obtained. The 2D and 3D inversion results gave same depths for each layer and exact positions of the anomalies along the imaging planes (survey lines). However, the 2D inversions gave lower resistivity values of the observed anomalies when compared with the resistivity values reported by the 3D inversions. These anomalies were folded onto the imaging planes and presented as anomalies along the planes. A comparison of the acquired field data set, the 2D and 3D inversion results showed that the 3D inversions gave better representations of each resistivity zones and clearly showed the resistivity variations of the various anomalies along and off the imaging planes with depths.

1. INTRODUCTION

Geoelectrical subsurface imaging is used to obtain the resistivity distribution underneath the earth's surface. This is done by measuring the resistance offered by the subsurface when current is sent into the ground with the aid of metallic electrodes called current electrodes. A measure of the resistance to the flow of electric

current by the subsurface material is known as the resistivity of that material. The ground resistivity is related to various geological parameters such as the mineral and fluid content, porosity and degree of water saturation in the rock. Geoelectrical subsurface imaging finds application in the study of inhomogeneous medium (Aigbogun et al., 2017), the determination of contaminants in environmental study (Olaseni et al., 2018), the determination of mineral deposit within the subsurface (Ogunlana et al., 2019) and the study of archaeological sites (Papadopoulos et al., 2006).

In a 2D inversion program, the earth is assumed to have a two-dimensional resistivity distribution, that is, any earth material on a 2D cross section under the survey line would have an infinite length along the direction normal to the survey line and any cross section parallel to the imaging section would look exactly the same. A round object on a 2D section would be an infinitely long cylinder in the earth. Mathematically, earth resistivity distribution can be expressed as a function of two spatial coordinates (x, z), i.e., $\rho = \rho(x, z)$. Since all geological structures are 3D in nature, i.e., $\rho = \rho(x, y, z)$, a fully 3D resistivity survey using a 3D interpretation model should in theory give the most accurate results (Dahlin and Loke, 1998; Olayinka, 1999; Olayinka and Yaramanci, 1999). In locations where the subsurface is inhomogeneous, the inversion results from the 2D resistivity surveys always comprise false geologic features as a result of 3D effects. This negates the 2D inversion conjecture that the resistivity distribution is 2D. This often leads to misrepresentation of the actual size and the exact location of the observed anomalies (Bentley and Gharibi, 2004). Another concern in 2D resistivity imaging methods is that the injected electric currents are not restricted to flow within the 2D imaging plane. The electric field has a 3D distribution. The anomalous objects off the imaging plane would also disturb the electric field and generate anomalies in the measurements and in the inverted resistivity image. The objects off the imaging plane would be folded onto the imaging plane and generate false anomalies.

Inversion of 3D data set produces a volume image showing 3D subsurface resistivity distribution. A 3D inversion program does not impose the constant resistivity restriction on the strike direction. The earth may have 3D arbitrarily structured resistivity distribution, which is a 3D function. Since all geological structures are 3D in nature, a fully 3D resistivity survey using a 3D interpretation model should in theory give the most accurate results. At the present time 3D surveys is a subject of active research. However, it has not reached the level where, like 2D surveys, it is routinely used. The main reason is that the survey cost is comparatively higher for a 3D survey of an area which is sufficiently large.

The 3D roll-along method has proven to be a useful tool for large survey area. Most commercial 3D surveys will probably involve grids of at least 16 by 16 in order to cover a reasonably large area. A 16 by 16 grid will require 256 electrodes which is more than that available on many multi-electrode resistivity meter systems. One method to survey such large grids with a limited number of electrodes is to extend the roll-along technique used in 2D surveys to 3D surveys (Dahlin and Bernstone, 1997). In this technique, to obtain a 3D data set, 2D data are acquired along parallel and orthogonal lines in a grid pattern (Dahlin and Loke, 1997). By this way, fewer number of electrodes, cables and time will be required for 3D data acquisition. Gharibi and Bentley (2005), reported that data acquired by the 3D roll along technique using the proper geometric constraints are suitable for processing and interpretation. An analysis of 3D resistivity surveys in the literature suggests that the 3D roll along approach is the most practical one among different techniques.

The aim of this research is to determine the similarities and differences between the two dimensional and three dimensional geoelectrical imaging based on the inversion results obtained from the study location and to ascertain which methods best suits the study location for the purpose of subsurface earth characterization.

2. MATERIALS AND METHODS

2.1. Study Location

The survey area, University of Benin Teaching Hospital (Figure 1) is located in the Ugbowo area of Edo State, Nigeria and lies within longitude 5º36'34" E, 5º36'43" E and latitude 6º23'23" N, 6º23'34" N. The geological arrangement in the area of study consists of the coastal plain sands sometimes referred to as Benin sands of the Benin Formation. The Benin Formation is assigned to the Oligocene-Pleistocene period in the continent of Africa and to the Oligocene-Pleistocene recent at the sub-oceanic. The formation consists of top reddish to reddish brown lateritic clayey sand overlaying permeable fresh water bearing sands, and sandstone with local thin clays and shale interbeds. Sands, sandstones and clays vary in colour from reddish brown to pinkish yellow on weathered surfaces to white in the deeper fresh surfaces. Limonitic coatings are responsible for the brown reddish-yellowish colour (Akujieze, 2004).

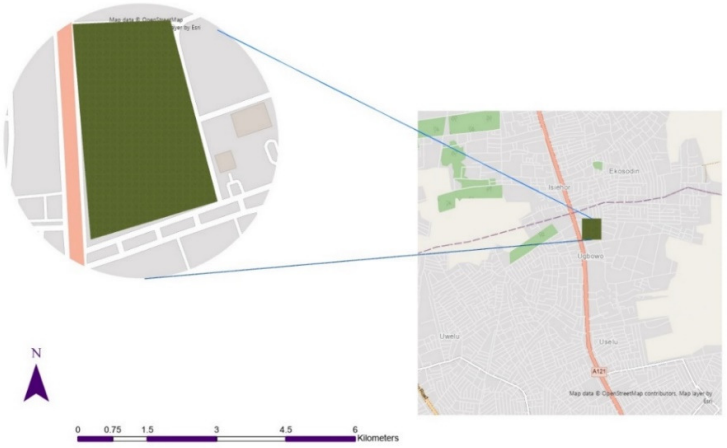

Figure 1: Geographic information system (GIS) showing the study location

2.2. Data Collection and Theoretical Background

The materials used for data acquisition include; the PASI Terrameter, battery, twenty-one (21) stainless steel electrodes, four (4) electrode connectors or clips, cables and reels, hammers, generating set, extension boxes, measuring tapes, GPS device, notebook, pen and umbrella. In order to study the electrical properties of the geologic features in the location, data were obtained along six (6) profiles; three (3) along the horizontal and three (3) along the vertical path of the location. A direction of W-E azimuth was adopted for the horizontal profiles 1, 2 and 3 and a S-N azimuth for the vertical profiles 4, 5, 6. as shown in Figure 2. The data collection was done using Wenner-Schlumberger array configuration. The choice of the configuration is largely because of its good signal-to-noise ratio and better horizontal coverage. The maximum depth of penetration of this array is greater than the Wenner array configuration (Loke, 2000). In this configuration, electric current is introduced into the subsurface using a pair of current electrodes (C1 and C2), placed at positions A and B. This current creates an electric field within the subsurface. The electric potential distribution due to this injected current is measured across a pair of potential electrodes (P1 and P2) at positions M and N as shown in Figure 3.

The resistance offered by the subsurface geologic feature is obtained by calculation using Ohm's law:

$$R = \frac{\Delta V}{I} \tag{1}$$

Where:

ΔV is the electric potential difference across the potential electrodes (P1 and P2)
I is the current introduced into the subsurface using a pair of current electrode (C1 and C2)

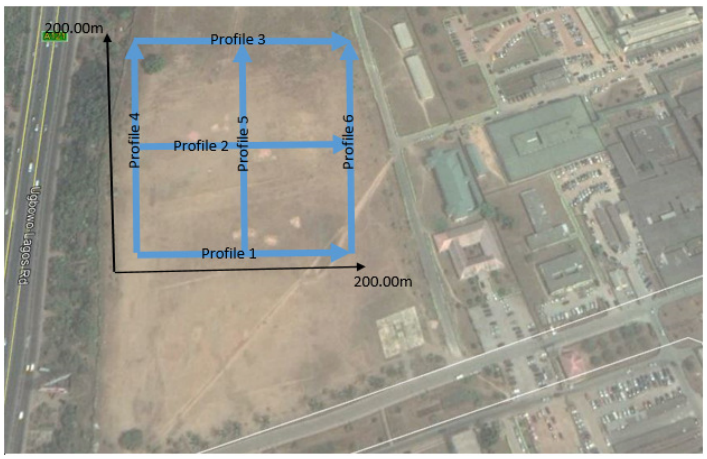

Figure 2: Google earth image showing the field design for the first location

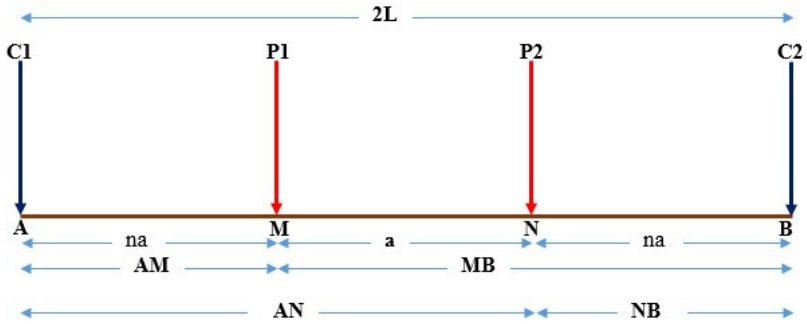

Figure 3: Electrode configuration adopted for the survey

The n factor is the ratio of the separation between the first current electrode (C1), and the first potential electrode (P1), or the second current electrode (C2), and the second potential electrode; P2, to the separation between the potential electrode pair. The potentials at the electrodes P1 and P2 are given as:

$$V_M = \frac{\rho I}{2\pi}\left[\frac{1}{AM} - \frac{1}{MB}\right] \; and \; V_N = \frac{\rho I}{2\pi}\left[\frac{1}{AN} - \frac{1}{NB}\right] \tag{2}$$

The potential difference, ($\Delta V_{MN} = V_M - V_N$), between the two potential electrodes is given as:

$$\Delta V_{MN} = V_M - V_N = \frac{\rho I}{2\pi}\left\{\left[\frac{1}{AM} - \frac{1}{MB}\right] - \left[\frac{1}{AN} - \frac{1}{NB}\right]\right\} = \frac{\rho I}{2\pi}\left\{\frac{1}{AM} - \frac{1}{MB} + \frac{1}{NB} - \frac{1}{AN}\right\} \tag{3}$$

The resistivity, (ρ), is obtained by rearranging Equation 3, and is given as:

$$\rho = \frac{2\pi \Delta V_{MN}}{I}\left\{\frac{1}{AM} - \frac{1}{MB} + \frac{1}{NB} - \frac{1}{AN}\right\}^{-1} \tag{4}$$

$$\rho = KR \tag{5}$$

$$Where \; K = 2\pi\left\{\frac{1}{AM} - \frac{1}{MB} + \frac{1}{NB} - \frac{1}{AN}\right\}^{-1} \; and \; R = \frac{\Delta V_{MN}}{I}$$

For this array type, the geometric factor; K is given as:

$$K = 2\pi\left\{\frac{1}{AM} - \frac{1}{MB} + \frac{1}{NB} - \frac{1}{AN}\right\}^{-1} = \pi\left(\frac{L^2}{a} - \frac{a}{4}\right) \tag{6}$$

Where a is the separation between the potential electrode pair (a = MN) and L is the average separation between the current electrode pair (C1 and C2) (L = AB/2).
The general expression for the geometric factor, K is:

$$K = \pi n\,(n+1)a \tag{7}$$

The electrodes were arranged along the profile lines which were 200 m long, each with a minimum electrode spacing of 10 m. Starting from the origin (first electrode), the output terminals of the current cables were connected to electrodes 1 and 4 and the input terminals of the potential cables were connected to electrodes 2 and 3 as shown in Figure 4. The input terminals of the current cables and the output terminals of the potential cables were connected to the Terrameter (Resistivity meter). The cables were moved along the profile lines, keeping the 10 m electrode spacing constant for the first traverse. After the first traverse, the first current and potential electrodes as well as the second current and potential electrodes were kept 20 m apart while the separation between the potential electrodes is kept constant at 10 m as shown in Figure 4. This implies that the current cables were connected to the first and sixth electrodes while the potential cables were connected to the third and fourth electrodes along the profile lines before the second traverse was taken.

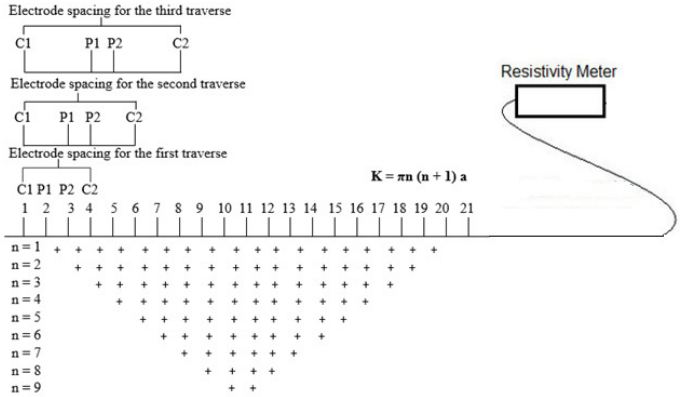

Figure 4: Current and potential electrode separations for each traverse

2.3. Data Analysis

The apparent resistivity for the two-dimensional (2D) survey obtained from each profile were computed by multiplying the resistance values with the geometric factors and then saved in a format that conform with the programs (RES2DINV and RES3DINV) used for the inversion process. The RES2DINV and RES3DINV programs are made to operate in an automatic and robust manner with little input from the user. They have sets of default parameters which guide the inversion processes. However, some of these parameters could be modified to fine tune the inversion process. Due to high resistivity near the ground surface, narrow model cell with width that is half the electrode spacing was adopted. This is done to improve the quality of the resolution. The 2D parallel and orthogonal data set were thereafter combined using a batch file to form a single 3D data set and inverted with the RES3DINV software. The 3D inversion result was exported to a Voxler software, where the 3D block model was computed. These processes are shown in Figure 5.

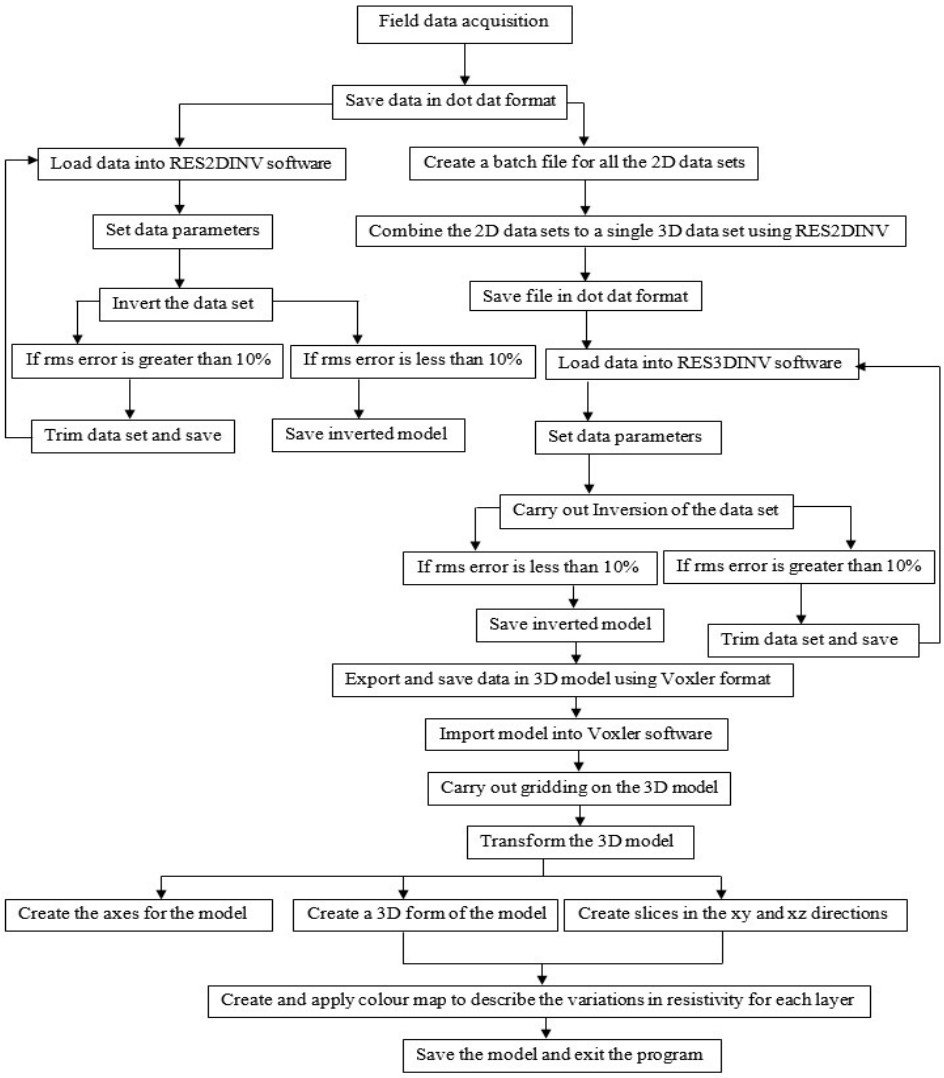

Figure 5: Data processing flow chat

3. RESULTS AND DISCUSSION

The 2D inversion model in Figure 6a showed a fairly resistive top layer that were almost uniform to a depth of 22.77 m with resistivity values of between 545 Ωm to 1184 Ωm. Other higher resistive zones of between 1330 Ωm to 6459 Ωm extended from a depth of about 22.77 m to about 39.60 m. The section of the 3D model in Figure 6b showed that resistivity values varied significantly along the imaging plane to a depth of about 22.70 m. The model showed an increase in resistivity within this depth from the end of the profile towards the origin, with resistivity values ranging from between 640 Ωm to 1184 Ωm. Below this inhomogeneous layer were series of high resistive homogeneous layers. The low resistive layers with resistivity values of between 640 Ωm to 750 Ωm observed between 0 m to 32 m, 45 m to 77 m and 90 m to 200 m appeared to extend through maximum and minimum distances of about 92 m and 22 m respectively, orthogonal to the imaging plane. Figures 6a and 6b showed inhomogeneity in resistivity distribution to a depth of about 22.77 m. Below this are high resistive layers which are uniformly distributed and the depths of each layer are clearly delineated. The low resistivity value of about 545 Ωm observed between 90 m to

110 m in Figure 6a differs from the value observed in Figure 6b to the same depth and positions. The minimum value observed is about 640 Ωm. The reason for the difference in these results is because the anomalies extended beyond the imaging planes as observed in the 3D results. In an attempted to capture the anomalies that were off these planes, the 2D inversions took these anomalies and merged them with the anomalies along the imaging plane, making it looks as if these anomalies were actually along the planes (Bentley and Gharibi, 2004; Yang and Lagmanson, 2006; Aizebeokhai, 2010).

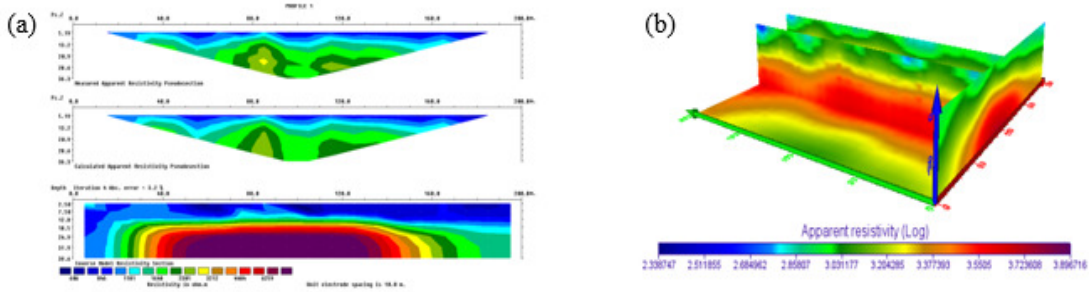

Figure 6: (a) 2D image and (b) 3D image for the first parallel profile

The 2D resistivity model in Figure 7a showed discontinuity in resistivity distribution along the profile, with resistivity values of between 511 Ωm to 1226 Ωm. The more resistive zone was between 70 m to 110 m along the profile. Due to the uneven distribution of resistivity along the profile, the depths of each resistive zones varied significantly. The 3D section in Figure 7b showed inhomogeneity in resistivity distribution in layer close to the surface with resistivity values ranging from 592 Ωm to about 1226 Ωm. The most resistive part of this layer was between 70 m to 110 m with a resistivity value of about 1226 Ωm. Low resistivity values of about 592 Ωm, 741 Ωm and 750 Ωm were visible between 184 m to 200 m, 126 m to 137 m and 45 m to 60 m respectively along the imaging plane. The depth of this layer also varied significantly along the imaging plane. The zone with resistivity of about 592 Ωm extends through a distance of about 28 m, orthogonal to the imaging plane.

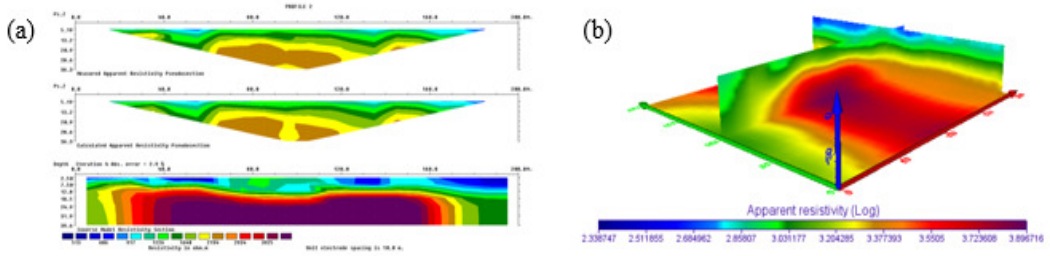

Figure 7: (a) 2D image and (b) 3D image for the second parallel profile

Figures 7a and 7b showed a maximum resistivity value of about 1126 Ωm within the inhomogeneous layer. Figures 7a and 7b showed minimum resistivity values of 511 Ωm and 592 Ωm respectively at the inhomogeneous layer. The reason for the difference in these results is because the anomalies extended beyond the imaging planes as observed in the 3D results. In an attempted to capture the anomalies that were off these planes, the 2D inversions took these anomalies and merged them with the anomalies along the imaging plane, making it looks as if these anomalies were actually along the planes (Aizebeokhai, 2010; Yang and Lagmanson, 2006; Bentley and Gharibi, 2004).

The 2D Inversion in Figure 8a showed slight variation in resistivity distribution with resistivity values varying with depth along the profile. The depth of the low resistive zone of about 314 Ωm was between 4.50 m and 14.70 m with distances of 40 m to 50 m and 150 m to 170 m respectively along the profile. Lower

resistive zone with resistivity value of approximately 230 Ωm, to a depth of about 8.38 m lie between 114 m to 150 m along the profile. The 3D section in Figure 8b showed resistivity values of 621 Ωm and 828 Ωm at distances of between 20 m to 93.50 m and 0 m to 20 m respectively, to a depth of about 7.50 m along the imaging plane. The 3D section also showed a lower resistivity zone of between 314 Ωm to 549 Ωm and at horizontal distances of between 108 m to 188 m which extended through distances of about 17.50 m and 65 m, orthogonal to the imaging plane. Figures 8a and 8b showed similarity in the depths of the inhomogeneous layer. The lowest resistivity values obtained at distances of between 118 m to 150 m were 230 Ωm and 314 Ωm respectively in Figure 8a and 8b. The reason for the difference in these results is because the anomalies extended beyond the imaging planes as observed in the 3D results. In an attempted to capture the anomalies that were off these planes, the 2D inversions took these anomalies and merged them with the anomalies along the imaging plane, making it looks as if these anomalies were actually along the planes (Aizebeokhai, 2010; Yang and Lagmanson, 2006; Bentley and Gharibi, 2004).

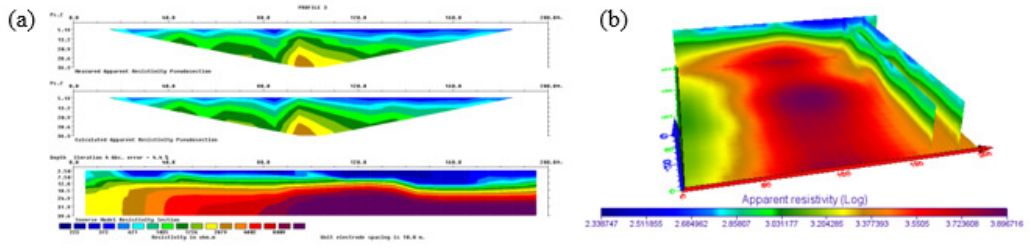

Figure 8: (a) 2D image and (b) 3D image for the third parallel profile

The 2D inverse resistivity model in Figure 9a showed inhomogeneity in resistivity distribution of the layer close to the surface to a depth of about 13.75 m. The resistivity values within this layer ranged from between 322.50 Ωm to 862 Ωm. The low resistive zone of between 322.50 Ωm to 550 Ωm was at distances of between 20 m to 77 m along the profile. Other resistive layers of higher resistivity values below this inhomogeneous layer appeared to be uniform along the profile. This section of the 3D model in Figure 9b showed inhomogeneity in resistivity distribution along the vertical. The variation was to a depth of about 13.75 m. This zone consisted of a resistivity value of between 490 Ωm to 550 Ωm at distances of between 28 m to 77 m along the imaging plane and extended to a distance of about 16 m, orthogonal to the imaging plane. The highest resistivity value within this depth was about 862 Ωm and was between 100 m to 140 m. The inhomogeneous layer observed in Figures 9a and 9b was to a depth of about 13.75 m. The inhomogeneous layer has a maximum resistivity of about 862 Ωm. There were variations in the lowest resistivity values recorded at distances of between 28 m to 77 m. Figures 9a and 9b showed resistivity values of 322.50 Ωm and 490 Ωm respectively. The maximum resistivity of about 862 Ωm was visible in both Figures 9a and 9b at distances of between 100 m to 140 m. The reason for the difference in these results is because the anomalies extended beyond the imaging planes as observed in the 3D results. In an attempted to capture the anomalies that were off these planes, the 2D inversions took these anomalies and merged them with the anomalies along the imaging plane, making it looks as if these anomalies were actually along the planes (Aizebeokhai, 2010; Yang and Lagmanson, 2006; Bentley and Gharibi, 2004).

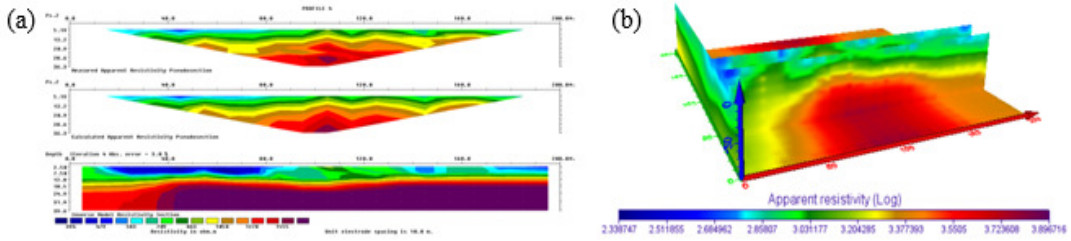

Figure 9: (a) 2D image and (b) 3D image for the first orthogonal profile

The 2D inversion in Figure 10a showed high resistive zones to a depth of 14.70 m from the surface. The highest resistivity value within this zone was about 1176 Ωm. The least resistive zone of about 340 Ωm, to a depth of about 7.50 m extended from the origin of the profile and terminated at a distance of about 12 m. The section of the 3D inversion in Figure 10b showed a high resistive subsurface. The highest resistivity value to a depth of about 14.70 m was 1176 Ωm and the lowest was 741 Ωm. It extended from the origin to about 12 m, orthogonal to the imaging plane. Figures 10a and 10b showed fairly homogeneous top layer with a maximum resistivity of about 1176 Ωm and to a maximum depth of 7.50 m. Figures 10a and 10b showed resistivity values of about 340 Ωm and 741 Ωm respectively from the origin to a distance of about 12 m. The reason for the difference in these results is because the anomalies extended beyond the imaging planes as observed in the 3D results. In an attempted to capture the anomalies that were off these planes, the 2D inversions took these anomalies and merged them with the anomalies along the imaging plane, making it looks as if these anomalies were actually along the planes (Aizebeokhai, 2010; Yang and Lagmanson, 2006; Bentley and Gharibi, 2004).

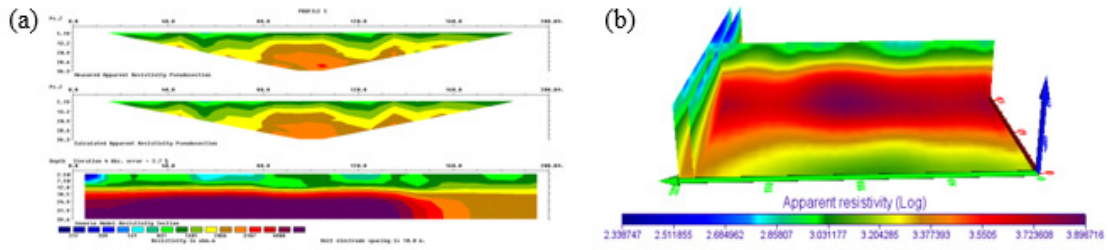

Figure 10: (a) 2D image and (b) 3D image for the second orthogonal profile

The 2D inversion in Figure 11a showed inhomogeneity in resistivity distribution along the profile. The most resistive layers appeared to taper out at a distance of 130 m from the origin along the profile. The zone with the least resistivity of between 270.50 Ωm to 394 Ωm lay between 67.78 m to 183 m. The 3D geoelectric section in Figure 11b showed a model with low resistive inhomogeneous zones. Resistivity values of between 484 Ωm to 727 Ωm spanned from the origin to a distance of 67.78 m. Low resistive zones with resistivity value of about 358 Ωm existed between 67.78 m to 183 m along the imaging plane but extended through a distance of about 20 m, orthogonal to the imaging plane. The most resistive parts of between 889 Ωm to 970 Ωm that made up this inhomogeneous region were observed at distances of between 190 m to 200 m along the imaging plane. The 2D inversion in Figure 11a and the 3D model in Figure 11b showed similarities in the positions of the low and high resistive zones within the homogeneous layer. The lowest resistive zone is between 67 m to 183 m while the higher resistive zone is between 190 m to 200 m. They however showed variations in the value of the lowest resistivity for the low resistive zone. The minimum resistivity values observed in Figures 11a and 11b are 270.50 Ωm and 358 Ωm respectively. The reason for the difference in these results is because the anomalies extended beyond the imaging planes as observed in the 3D results. In an attempted to capture the anomalies that were off these planes, the 2D inversions took these anomalies and merged them with the anomalies along the imaging plane, making it looks as if these anomalies were actually along the planes (Aizebeokhai, 2010; Yang and Lagmanson, 2006; Bentley and Gharibi, 2004).

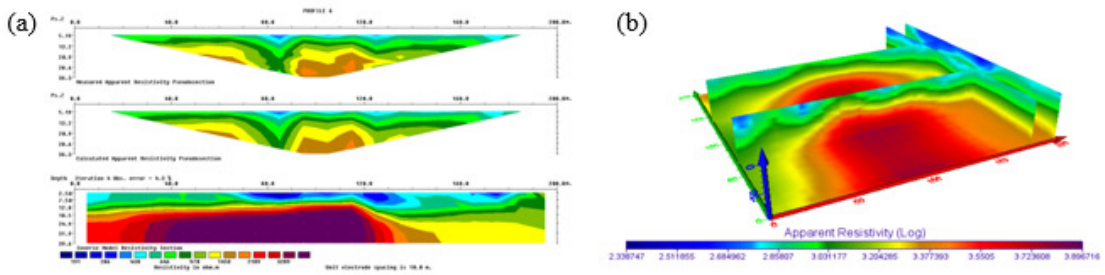

Figure 11: (a) 2D image and (b) 3D image for the third orthogonal profile

4. CONCLUSION

The results of the two dimensional and 3D surveys showed subsurface layers that were clearly delineated. The inversion results obtained from the 2D survey showed similarities with the inversion results of the 3D survey. They both reported same depths for each layer including that of the anomalies encountered in the inhomogeneous zone and the maximum resistivity values for each layer. The difference between the 2D and 3D inversions was their representations of the anomalies. The 2D inversion, in an attempt to report the actual variation in resistivity of the subsurface gave false representations of the anomalies along the imaging planes. This was because anomalies that were off the imaging planes were forced onto the planes, thus making the zones that contain the anomalies less resistive when compared with the resistivity values reported by the 3D inversion. The 3D inversions gave better results of each resistivity zones and clearly showed the resistivity variations along the parallel and orthogonal paths with depths. The degree of the variations in the lowest resistivity values reported within the inhomogeneous layers by the 2D and 3D inversions could depend largely on the extent of the spread of the anomalies along the parallel and orthogonal directions. In spite of this shortcoming associated with 2D surveys, it is still a viable tool for mapping out the approximate positions and depths within the survey area. For better understanding of the nature and spread of the anomalies, 3D survey is the best tool for this study location.

5. ACKNOWLEDGMENT

The authors wish to acknowledge the assistance and contributions of the Management and Staff of the University of Benin Teaching Hospital, Benin City, Nigeria for allowing us use their premises for this study.

6. CONFLICT OF INTEREST

There is no conflict of interest associated with this work.

REFERENCES

Aigbogun, C.O., Alile, O.M. and Egbai, J.C. (2017). Geoelectrical Imaging for Shallow Site Investigation at Ekiugbo in Uhunmwode Local Government Area of Edo State, Nigeria. *Journal of Applied Sciences and Environmental Management,* 21 (5), pp. 873-876.

Aizebeokhai, A. P. (2010). 2D and 3D geoelectrical resistivity imaging: Theory and field design. *Scientific Research and Essays*, 5(23), pp. 3592-3605.

Akujieze, C. N. (2004). Effects of Anthropogenic Activities (Sand Quarrying and Waste Disposal) on Urban Groundwater System and Aquifer Vulnerability Assessment in Benin City, Edo State, Nigeria. PhD Thesis, University of Benin, Benin City, Nigeria.

Bentley, L. R. and Gharibi, M. (2004). Two- and three-dimensional electrical resistivity imaging at a heterogeneous site. *Geophysics*, 69, pp. 674-680.

Dahlin, T. and Bernstone, C. (1997). A roll-along technique for 3D resistivity data acquisition with multi-electrode arrays. *Proceedings SAGEEP'97, Reno, Nevada,* pp. 927-935.

Dahlin, T. and Loke, M. H. (1998). Resolution of 2D Wenner resistivity imaging as assessed by numerical modeling. *Journal of Applied Geophysics*, 38, pp. 237-249.

Dahlin, T. and Loke, M. H. (1997). Quasi-3D resistivity imaging-mapping of three-dimensional structures using two-dimensional DC resistivity techniques. *Proceedings of the 3rd Meeting of the Environmental and Engineering Geophysics Society*, pp. 143-146.

Gharibi, M. and Bentley, L. R. (2005). Resolution of 3-D electrical resistivity images from inversions of 2-D orthogonal lines. *Journal of Environmental and Engineering Geophysics*, 10, pp. 339–349.

Loke, M. H. (2000). Electrical imaging surveys for environmental and engineering studies: A practical guide to 2-D and 3-D surveys. *http://www.terrajp.co.jp/lokenote.pdf*.

Ogunlana, O.F., Alile, O.M. and Airen, O.J. (2019). Two-dimensional Electrical Resistivity Tomography of Bitumen Occurrence in Agbabu, Southwest Nigeria. *Current Journal of Applied Science and Technology*, 36(1), pp. 1-9.

Olaseni, V. B., Onifade, Y. S., Airen, J. O., and Alile, O. M. (2018). Geoelectrical Subsurface Imaging for the Mapping of Leachate and Contaminant Plume around Septic Tanks Within the Staff Quarters in University of Benin, Benin City, Nigeria. *Asian Journal of Physical and Chemical Sciences*, 5(4), pp. 1-10.

Olayinka, A. I. (1999). Advantage of two-dimensional geoelectrical imaging for groundwater prospecting: case study from Ira, southwestern Nigeria. *Journal of the Nigerian Association of Hydrogeologists,* 10, pp. 55-61.

Olayinka, A. I. and Yaramanci, U. (1999). Choice of the best model in 2-D geoelectrical imaging: case study from a waste dump site. *European Journal Environmental Engineering Geophysics,* 3, pp. 221-244.

Papadopoulos, N. G., Tsourlos, P., Tsokas, G. N. and Sarris, A. (2006). Two-dimensional and Three-dimensional Resistivity Imaging in Archaeological Site Investigation. *Archaeology Prospect*, 13, pp. 163–181.

Yang, X. and Lagmanson, M. (2006). Comparison of 2D and 3D Electrical Resistivity Imaging Methods. *Conference Proceedings, 19th EEGS Symposium on the Application of Geophysics to Engineering and Environmental Problems*, cp-181-00057.